

# Distributed Quantum Approximate Optimization Algorithm on Integrated High-Performance Computing and Quantum Computing Systems for Large-Scale Optimization

Seongmin Kim<sup>1</sup>, Tengfei Luo<sup>2</sup>, Eungkyu Lee<sup>3</sup>, and In-Saeng Suh<sup>1</sup>

<sup>1</sup>National Center for Computational Sciences, Oak Ridge National Laboratory, Oak Ridge,  
Tennessee 37830, United States

<sup>2</sup>Department of Aerospace and Mechanical Engineering, University of Notre Dame, Notre  
Dame, Indiana 46556, United States

<sup>3</sup>Department of Electronic Engineering, Kyung Hee University, Yongin-Si, Gyeonggi-do 17104,  
Republic of Korea

## Abstract

Quantum approximated optimization algorithm (QAOA) has shown promise for solving combinatorial optimization problems by providing quantum speedup on near-term gate-based quantum computing systems. However, QAOA faces challenges in optimizing variational parameters for high-dimensional problems due to the large number of qubits required and the complexity of deep circuits, which limit its scalability for real-world applications. In this study, we propose a distributed QAOA (DQAOA), which leverages a high-performance computing-quantum computing (HPC-QC) integrated system. DQAOA leverages distributed computing strategies to decompose a large job into smaller tasks, which are then processed on the HPC-QC system. The global solution is iteratively updated by aggregating sub-solutions obtained from DQAOA, allowing convergence toward the optimal solution. We demonstrate that DQAOA can handle considerably large-scale optimization problems (e.g., 1,000-bit problem) achieving high accuracy ( $\sim 99\%$ ) and short time-to-solution ( $\sim 276$  s). To apply this algorithm to material science, we further develop an active learning algorithm integrated with our DQAOA (AL-DQAOA), which involves machine learning, DQAOA, and active data production in an iterative loop. We successfully optimize photonic structures using AL-DQAOA, indicating that solving real-world optimization problems using gate-based quantum computing is feasible with our strategies. We expect the proposed DQAOA to be applicable to a wide range of optimization problems and AL-DQAOA to find broader applications in material design.

**Keywords:** HPC-QC integration, large-scale optimization, quantum approximate optimization algorithm, gate-based quantum computing, distributed computing, active learning, material design, high-performance computing

## 1. Introduction

Quantum computing, leveraging quantum phenomena such as superposition and entanglement, significantly advances computational capabilities, promising to solve complex problems that classical computing finds intractable [1, 2, 3, 4, 5, 6]. This transformative technology harnesses the principles of quantum mechanics to process information in fundamentally new ways, revolutionizing various fields including cryptography, materials science, and artificial intelligence [7, 8, 9, 10, 11]. Researchers are increasingly utilizing quantum computing to accelerate their work across various domains [12, 13]. In particular, the quantum approximate optimization algorithm (QAOA) [14], a variational quantum algorithm employing both classical and quantum computing to optimize a cost function by iteratively adjusting parameters in both classical and quantum components (Fig. 1a), has demonstrated significant potential in efficiently tackling complex optimization problems, potentially providing quantum advantage [15, 16, 16, 17]. For example, a recent study by Shaydulin et al. has verified that QAOA can outperform the best-known classical solver for specific optimization problems [18]. Furthermore, other researchers have also applied this quantum algorithm to various combinatorial optimization problems such as the traveling salesman problem, the max-cut problem, and the knapsack problem, demonstrating the potential advantages of leveraging quantum computing [19, 20, 21].

The performance of QAOA has been improved through various strategies, such as advanced ansatz preparation, optimized initialization parameters, and optimized number of layers [22, 23]. However, the current era of quantum computing, known as a noisy intermediate-scale quantum (NISQ) era, presents several challenges. The biggest challenge is that current quantum computing systems, including quantum devices and quantum simulators, are characterized by a limited number of qubits and can only solve problems representing shallow quantum circuits [24, 25, 26]. These limitations make it challenging to scale up to real-world problems (e.g., optimization of photonic structures), which generally require a large number of qubits to represent high-dimensional binary spaces with deep circuits. Consequently, most QAOA studies involve small problems requiring only a few to tens of qubits [27, 19, 28]. For example, Kim et al. demonstrated that QAOA running with Qiskit Aer simulators exhibits low accuracy and long computation times for problems requiring more than 28 qubits, highlighting its difficulty in solving large-scale optimization problems [29].

To address the noise and error challenges in the NISQ era, the research community is exploring hybrid architectures that integrate high-performance computing (HPC) with quantum computing (QC). Here, HPC systems distribute a large task into numerous sub-

tasks through distributed computing across multi-cores/nodes, and distributed tasks can be efficiently handled by QC with appropriate sizes. This HPC-QC integrated system can potentially overcome limitations from current quantum systems by distributing heavy workloads and optimizing the use of quantum resources. Consequently, the HPC-QC integrated system can enhance the overall computational capability by leveraging the strengths of both technologies [30, 31, 27]. However, there has been a lack of research on integrating HPC and QC to solve large-scale optimization problems that require hundreds of qubits.

In this work, we develop a distributed QAOA (DQAOA) leveraging an HPC-QC integrated system to efficiently solve real-world optimization problems featuring large-scale models. Our algorithm achieves apparently higher accuracy ( $\sim 99\%$ ) and is significantly faster (over 160 times) at solving optimization problems (e.g., optimizing metamaterial structures). Furthermore, our approach enables us to efficiently solve large-scale problems (e.g., 1,000-bit problem) while conventional quantum computing approaches find difficulties in solving even much smaller problems (e.g., 30-bit problem). We further propose an active learning algorithm working with the proposed DQAOA for material design. We successfully apply this algorithm to optimize high-performance photonic structures, demonstrating the capability to solve real-world large-scale problems with gate-based quantum computing. By combining the distributed computing capability of HPC with the advantage of QC, our approach aims to tackle the challenges in the NISQ era, paving the way for practical and effective applications of QC in solving complex and large-scale problems. It is important to note that we utilize conventional quantum algorithms and systems, highlighting that the performance of our algorithm can be further improved by employing advanced algorithms and systems. Therefore, our algorithm not only addresses the limitations of current quantum techniques but also sets a foundation for future advancements as quantum technology continues to evolve.

## 2. Results and Discussion

### 2.1 Distributed QAOA

Combinatorial optimization problems, known as nondeterministic polynomial-time (NP)-hard problems, can be represented as quadratic unconstrained binary optimization (QUBO) problems, which can serve as Hamiltonians for QAOA [32, 33, 34, 35]. Although QAOA has shown potential for speedup in solving QUBO problems, the limited number of qubits in current quantum systems and the deep circuit depth required for representing large-scale problems (Fig. 1b) present challenges for solving real-world problems in the NISQ era [24, 25, 29]. To address these challenges, we decompose a large QUBO (size of  $n$ ) into smaller sub-QUBOs (size of  $k$ ), and solve them through the proposed DQAOA. Here, multi-cores/nodes on HPC systems are employed to solve each sub-QUBO through distributed parallel computing. A global solution  $\mathbf{x}_g$  is obtained by aggregating sub-solutions

$s$  (from  $s_1$  to  $s_b$ , obtained from each sub-task, where  $b$  indicates the number of sub-QUBOs). The energy of the large QUBO with a global solution ( $\mathbf{Q}_g$ ) is calculated, and the  $i^{\text{th}}$  decision variable of a global solution  $x_{g,i}$  is updated if  $\mathbf{Q}_g$  decreases by changing the decision variable to that of a sub-solution  $s_{l,i}$  (i.e.,  $\mathbf{Q}_{g,s_{l,i}} < \mathbf{Q}_{g,x_{g,i}}$ , Fig. 1c). We first initialize a global solution by solving initial sub-QUBOs that are decomposed with a linear order from the first to the last decision (Fig. S1a). This process ensures that every decision is visited at least once by any sub-QUBO. After that, the original large QUBO is decomposed again into  $b$  sub-QUBOs with randomly selected decision variables (according to the sub-QUBO size,  $k$ ) for DQAOA (Fig. S1b). After solving the sub-QUBOs on different cores and nodes using QAOA, the global solution is updated based on the calculated energy ( $\mathbf{Q}_g$ ). Additionally, we manually flip the first and last decisions to evaluate the energy of QUBO with the changed binary vector. Iterating these processes improves the quality of the global solution, converging toward a (quasi) optimal solution (Fig. 1c). We note that this algorithm, which integrates classical computing with quantum computing, can work on multi-cores/nodes as well as a single core. QAOA working with a decomposed QUBO on a single core is noted as "dq-QAOA" (decomposed QUBO with QAOA), and it handles a single sub-QUBO without distribution (i.e., the number of sub-QUBO,  $b$  in the iteration step, is 1). However, it requires many iterations to achieve a high-quality solution in this case. On the other hand, DQAOA running on multi-cores/nodes HPC systems can solve multiple sub-QUBOs in one iteration through distributed parallel computing ( $b \gg 1$ ), thus requiring significantly fewer iterations to obtain a high-quality solution. For DQAOA, initialization requires at least  $n-k+1$  cores to assign each task (i.e., solving each sub-QUBO) to each core while  $n$  is usually much larger than  $k$ . Hence, we use more than  $n$  cores to solve a problem size of  $n$  (i.e.,  $n$ -bit problem) for DQAOA (see the Method section for more details).

## 2.2 Performance Analysis of DQAOA

We use the Qiskit Aer simulator with the 'automatic' method for quantum circuits due to its highest accuracy and fastest time-to-solution for QAOA [29], as seen in Fig. S2 (information about evaluating accuracy and time-to-solution is in Supplementary Information). Despite its high performance, the accuracy decreases, and time-to-solution exponentially increases as a problem size ( $n$ ) increases. Hence, it is hard to solve even 30-bit problems ( $n=30$ ) using QAOA with this quantum system. It should be noted that we do not propose a new QAOA algorithm or a new quantum simulator to improve their performances. Instead, we propose a strategy that employs the HPC-QC integrated system based on the conventional algorithm and system to scale the problem sizes while achieving high accuracy and reduced time-to-solution. First, we analyze the performance of dq-QAOA for a 30-bit problem, which requires many iterations as it does not leverage distributed computing. Fig. 2a shows that increasing the number of iterations allows for achieving higher accuracy, but the accuracy almost converges after 300 iterations. Notably, more

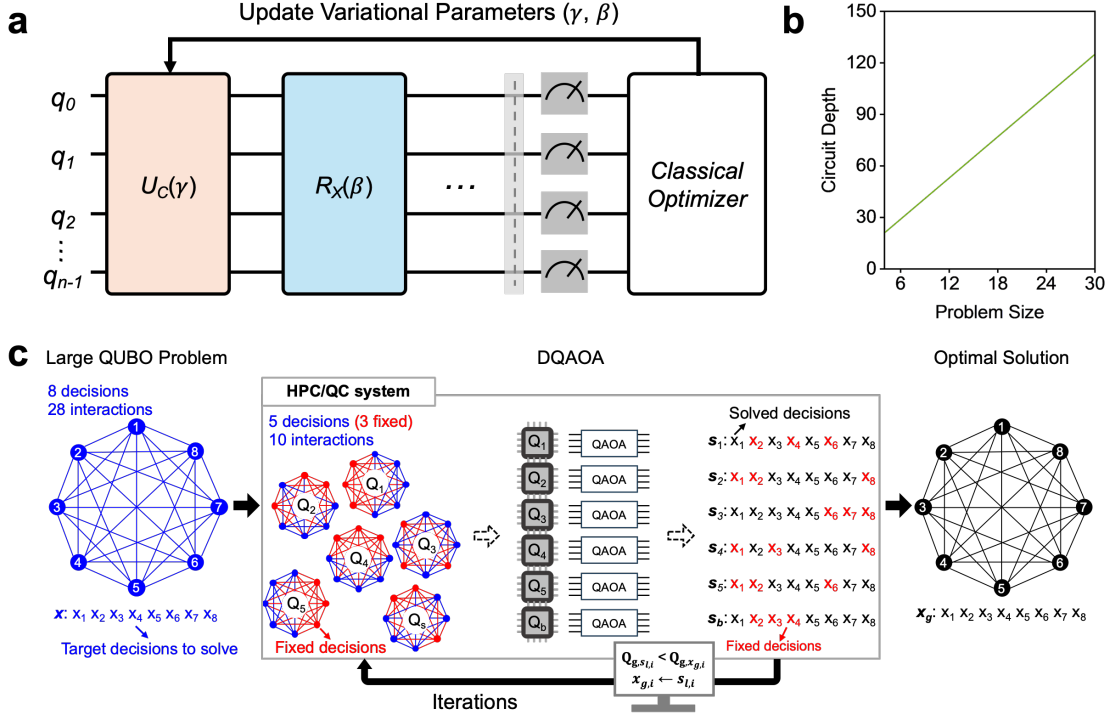


**Fig. 1: Workflow of DQAOA leveraging an HPC-QC integrated system.** **a.** The schematic of a QAOA circuit, illustrating the iterative process to update variational parameters in both classical and quantum components. **b.** Circuit depth as a function of a QUBO problem size, showing that the circuit depth increases for larger problems, which indicates the difficulty in solving large-scale problems. **c.** The schematic of DQAOA to solve large-scale optimization problems through distributed computing. A large QUBO is decomposed into  $b$  sub-QUBOs, which are solved by the HPC-QC integrated system.

iterations continue to increase time-to-solution, thus the optimal number of iterations is set to 300 for the rest of the studies unless otherwise noted. We further investigate the performance of dq-QAOA with larger sub-QUBO sizes (from 4 to 10). The accuracy does not significantly improve with the larger sizes while time-to-solution exponentially increases due to the increasing number of qubits required and deeper circuits for solving larger sub-QUBOs (Figs. 2b and S2b). Therefore, we use these hyperparameters (the number of iterations of 300 and the sub-QUBO size of 4) for dq-QAOA. As seen in Fig. 2c, QAOA already exhibits a low accuracy for  $n=30$  ( $\sim 84\%$ ) while dq-QAOA has a much higher accuracy ( $\sim 95\%$ ). Furthermore, time-to-solution exponentially scales with QAOA while it linearly increases with dq-QAOA, making it several orders of magnitude faster than QAOA (Fig. 2d). Nevertheless, dq-QAOA yields low accuracies for even larger problems ( $n \geq 50$ ), thus we tune the hyperparameters to verify if higher accuracies can be achieved. Figs. 2e and 2f confirm that increasing the number of iterations and increasing the sub-QUBO size help improve the accuracies for such large problems ( $\sim 91\% \rightarrow \sim 97\%$  for  $n=50$ , and  $\sim 69\% \rightarrow \sim 83\%$  for  $n=150$ ). However, the time-to-solution greatly increases ( $\sim 69$  s  $\rightarrow \sim 2,475$  s for  $n=50$ , and  $\sim 97$  s  $\rightarrow \sim 2,417$  s for  $n=150$ ), which demands further improvement for the practical application of this algorithm to solve real-world

problems.

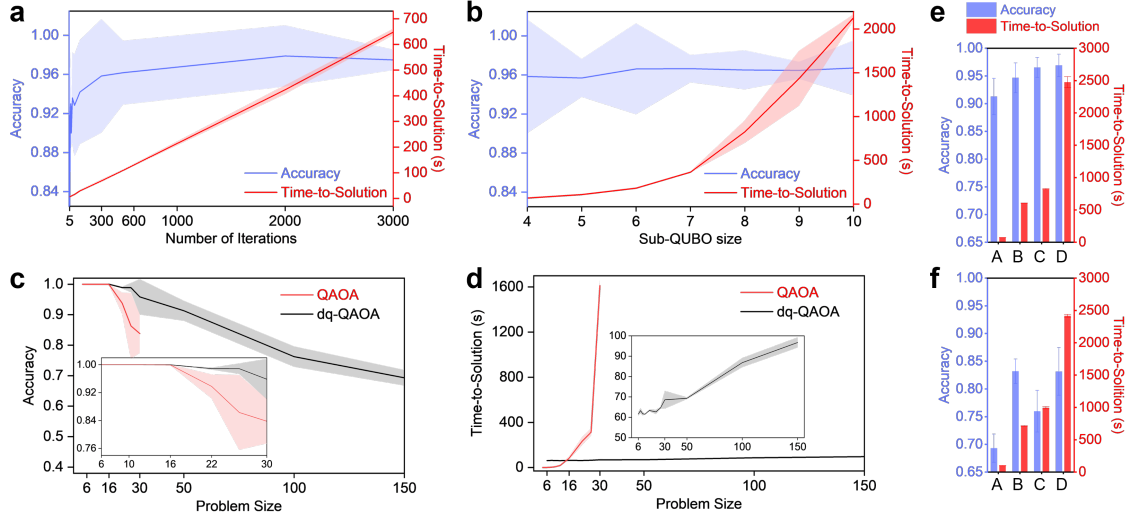


**Fig. 2: Performance analysis of dq-QAOA.** Accuracy and time-to-solution for a 30-bit problem as a function of (a) the number of iterations, and (b) the sub-QUBO size. The number of iterations is set to 300 and sub-QUBO size to 4 for further studies, as accuracy nearly converges but time-to-solution continues to increase. (c) Accuracy and (d) time-to-solution of QAOA and dq-QAOA as a function of the problem size. Accuracy and time-to-solution of dq-QAOA for a problem size of (e) 50 and (f) 150 with different number of iterations and sub-QUBO sizes. **A:** 300 iterations with the sub-QUBO size of 4. **B:** 3,000 iterations with the sub-QUBO size of 4. **C:** 300 iterations with the sub-QUBO size of 8. **D:** 1,000 iterations with the sub-QUBO size of 8.

DQAOA performs remarkably better than dq-QAOA and QAOA with significantly higher accuracy and reduced time-to-solution. Fig. 3a indicates that DQAOA achieves a high accuracy ( $\sim 95\%$ ) and short time-to-solution ( $\sim 13$  s), needing only 30 iterations, for a large problem ( $n=150$ ). On the other hand, dq-QAOA shows a lower accuracy ( $\sim 83\%$ ) with much longer time-to-solution ( $\sim 2,417$  s) even after the hyperparameter tuning. This notable acceleration in solving the large problem is attributed to distributed parallel computing, which allows the HPC-QC integrated system to handle many sub-QUBOs across multi-cores/nodes simultaneously. Furthermore, this approach enables updating the global solution more times with a larger number of sub-QUBOs, resulting in higher accuracy. Employing even more cores and nodes allows more number of sub-QUBOs ( $b$ ) for each iteration, possibly leading to obtaining a higher-quality global solution. However, Fig. 3b presents that using cores more than the problem size does not greatly improve the accuracy, but increases time-to-solution due to the communication overheads between cores and nodes. In addition, Fig. S3 reveals that increasing a sub-QUBO size (4 to 8) leads to a slightly higher accuracy but increases time-to-solution quite significantly. Hence, we set the number of iterations to 30, the sub-QUBO size to 4, and the number of cores used equal to the problem size ( $n$ ). Given these hyperparameters, DQAOA demonstrates a strong capability to scale problem sizes ( $n=6$  to 1,000). DQAOA exhibits a high accuracy ( $\sim 99\%$ ) and short time-to-solution ( $\sim 276$  s) even for a very large problem

( $n=1,000$ ), while QAOA and dq-QAOA cannot handle it (Figs. 3c and 3d). Fig. S4 presents the comparison of accuracy and time-to-solution between QAOA, dq-QAOA, and DQAOA for various problem sizes. The results clearly show that DQAOA exhibits the best accuracy compared to that of QAOA and dq-QAOA (Fig. S4a). Furthermore, DQAOA is  $>160$  times and  $>7$  times faster than QAOA and dq-QAOA, respectively (Fig. S4b). More importantly, DQAOA can further scale problem sizes (over 150), which QAOA and dq-QAOA cannot handle. Note that QUBOs used for this study representing real-world problems are large and dense (Fig. S5), and only DQAOA can solve such large and dense QUBO problems highly efficiently. These performance analysis results demonstrate the superior performance of DQAOA, leveraging the HPC-QC integrated system for distributed computing, in solving large-scale optimization problems, which are intractable with the conventional QAOA. In addition, we expect that the performance of DQAOA can be further improved by employing advanced QAOA algorithms and quantum systems, which is beyond the scope of this study.

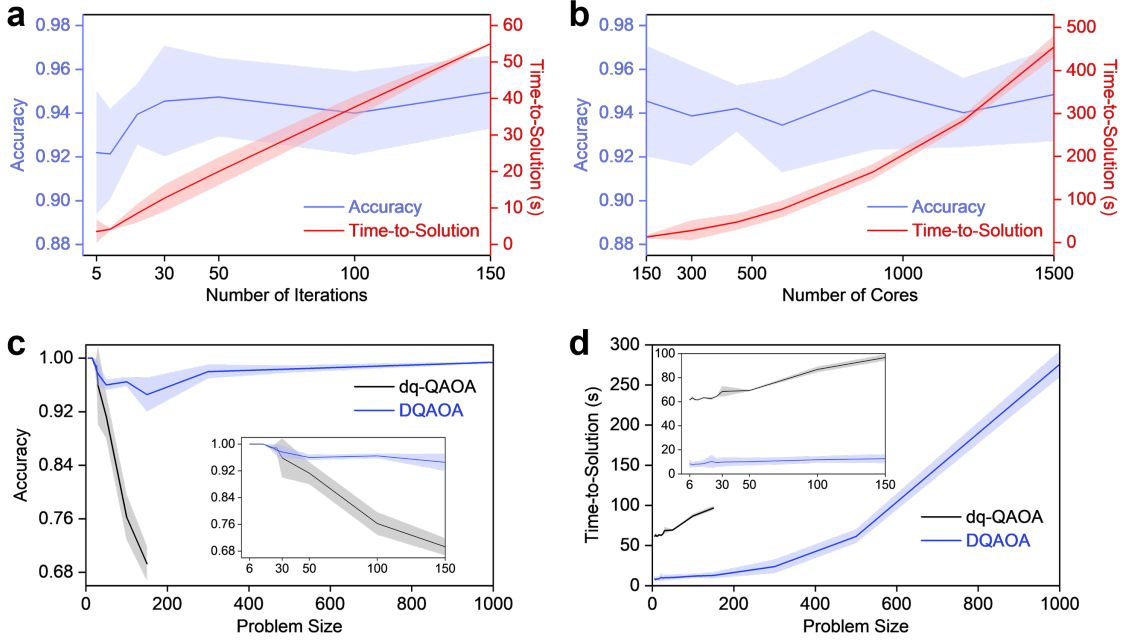


**Fig. 3: Performance analysis of DQAOA.** Accuracy and time-to-solution for a 150-bit problem as a function of (a) the number of iterations, and (b) the number of cores used. (c) Accuracy and (d) time-to-solution of dq-QAOA and DQAOA as a function of the problem size ( $n$ ). Note that the number of iterations, sub-QUBO size, and the number of cores used for DQAOA are set to 30, 4, and  $n$ , respectively.

## 2.3 Active Learning with DQAOA for Real-World Optimization Problems

We further develop an active learning algorithm working with our DQAOA (AL-DQAOA) for optimizing material structures (layered metamaterials for spectral filters), featuring

complex and large optimization spaces. This AL-DQAOA integrates machine learning, our DQAOA, and wave-optics simulation in an iterative loop (Fig. 4a). Here, a machine learning model (factorization machine, FM) is used to generate a QUBO as a surrogate, describing the relationship between material structures and their figure-of-merits (FOMs) [36, 37]. Then, DQAOA solves the given QUBO problem to predict an optimal state that represents an optimal material structure ( $\mathbf{x}_{po}$ ). Subsequently, optical properties are evaluated by wave-optics simulation to calculate an FOM of the identified material structure ( $FOM_{po}$ ). Finally, the dataset previously used for FM training is updated by including  $\mathbf{x}_{po}$  and  $FOM_{po}$ . Iterations of these processes (noted as optimization cycles) improve the dataset quality and refine QUBO surrogates, gradually converging toward the optimal state in the global optimization space. It should be noted that this algorithm is designed for minimization optimization problems, where materials with lower FOMs yield higher performances (see the Method section for more details).

We apply AL-DQAOA to optimize spectral filters with complex optical properties depending on the wavelength of the incident light, which can be used as a transparent radiative cooler (TRC) for window applications (Figs. 4b and 4c, see the Method section for more details). AL-DQAOA can effectively find the optimal structure in a global optimization space for a 6-layered structure (12-bit optimization problem), as shown in Figs. 4d and S6. More iterations are required for larger optimization spaces, generally achieving convergence within several thousands of optimization cycles (Figs. 4d and S7). Here, the optimization time per cycle for 12, 30, 50, and 100-bit systems is 13, 20, 29, and 35 s, respectively, with the simulation time using the transfer matrix method (TMM) being less than 0.1 s (Fig. 4e) [38]. Note that DQAOA takes 7 to 10 s and the total time required for completing optimization of 12, 30, 50, and 100-bit systems are respectively  $\sim 0.9$ ,  $\sim 11.1$ ,  $\sim 32.9$ , and  $\sim 48.9$  hours, which should be much faster than AL with dq-QAOA (AL-dq-QAOA). To further demonstrate the superior performance of DQAOA, we optimize the same systems using dq-QAOA instead of DQAOA within AL. The results show that optimization using AL-dq-QAOA results in higher FOMs (indicating lower performances) and longer optimization times since dq-QAOA has lower accuracy and takes longer in solving given QUBOs than DQAOA (Figs. S8 and S9), which agree well with our performance analysis study in Figs. 2 and 3. These results highlight the benefit of using DQAOA within the AL algorithm not just for reducing optimization time but also for identifying high-performance materials.

The optimal structure identified by AL-DQAOA has a low FOM of 0.5208 (Fig. 4d). Hence, as shown in Fig. 4f, the optimized material exhibits desired optical properties close to the ideal one (high transmitted solar irradiance in the visible range and low in the ultraviolet/near-infrared ranges). Furthermore, due to the thermal radiative layer on the top, this material yields high emission efficiency in the mid/long infrared range (Fig. S10) [39]. These distinct optical properties can lead to energy-saving capability for cooling by reflecting heat-generating photons and emitting thermal radiation through

the atmospheric window while transmitting visible light [40, 33]. Thus, it can be used for TRC windows, which have attracted a lot of attention recently in addressing the global warming issue [41, 42]. We calculate the energy-saving capability when using this optimized material for windows (see more details in Supplementary Information). The calculation results reveal that the optimized spectral filter used as TRC windows can save cooling energy consumption by up to  $\sim 34.3\%$  compared to conventional windows (Figs. 4g and S11). The results demonstrate that AL-DQAOA allows for systematic design and optimization, leveraging the capabilities of both HPC and QC, contributing to the development of high-performance materials with complex, large optimization spaces.

### 3. Conclusion

In this work, we have developed DQAOA leveraging the integrated HPC-QC system to solve large-scale, real-world optimization problems based on conventional quantum algorithms and conventional quantum computing systems. Our performance analysis demonstrates that DQAOA achieves high accuracy and significantly reduces time-to-solution by employing distributed computing across multi-cores and nodes on the HPC-QC integrated system. Consequently, DQAOA can effectively handle extensive problems, such as a 1,000-bit problem, achieving an accuracy of  $\sim 99\%$  and time-to-solution of  $\sim 276$  s, which conventional methods may find challenging to solve. Furthermore, we have proposed AL-DQAOA, an optimization algorithm aiming to optimally design material structures leveraging gate-based quantum computing. This algorithm successfully optimizes photonic structures (spectral filters for TRC as examples), which represent 100-bit real-world optimization problems. Importantly, AL-DQAOA performs much more accurately and faster in identifying optimal structures compared to AL-dq-QAOA. This suggests utilizing DQAOA within AL for material design tasks if HPC-QC integrated systems are available. We present the optical properties of the optimized functional material, which resembles the ideal one, and demonstrate the energy-saving potential of the optimized material. We expect that the proposed DQAOA working with HPC-QC integrated systems can be generalized to various optimization tasks, such as finance, routing, scheduling, and assignment. In addition, the proposed AL-DQAOA will be useful for material design in general. Future enhancements could include adopting advanced quantum algorithms and computing systems to further optimize DQAOA's performance and expand AL-DQAOA's applicability in material design and beyond.

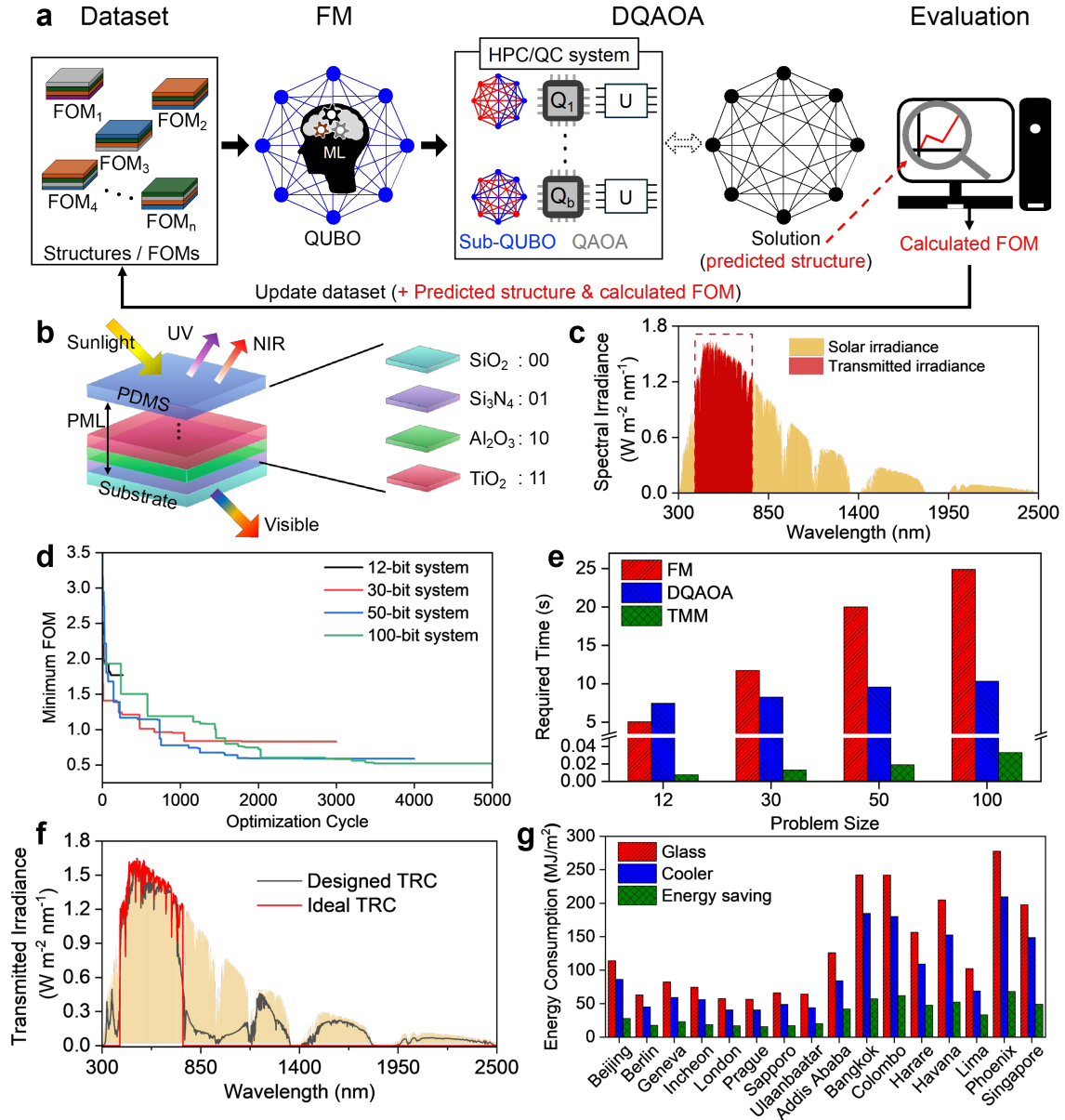


**Fig. 4: The AL-DQAOA algorithm for solving large-scale optimization problems in material science, exemplified by spectral filters with 12, 30, 50, and 100-bit systems.** **a.** The schematic of AL-DQAOA integrating machine learning, DQAOA, and performance evaluation in an iterative loop. **b.** The schematic of a spectral filter for TRC windows, where the planar multilayered structure (PML) is subject to optimization. **c.** Solar spectral irradiance (yellow shade, air mass 1.5 global) and transmitted irradiance through the ideal spectral filter (red shade). The ideal spectral filter transmits the solar spectrum only in the visible range. **d.** The evolution of FOM as a function of optimization cycles for different problem sizes. **e.** Time required for an optimization cycle of AL-DQAOA for different problem sizes. **f.** Calculated optical properties of the spectral filter optimized by AL-DQAOA. The yellow shade presents solar spectral irradiance. **g.** Energy-saving potential when using the optimized spectral filter as TRC windows in cities around the world, compared to a conventional window.

## 4. Methods

### 4.1 QUBO - Representing Optimization Problems

In the field of quantum computing, variational quantum algorithms have shown great promise in efficiently addressing optimization problems, particularly when formulated with QUBO models. Then, the quantum systems rapidly identify an optimal binary state ( $\bar{\mathbf{x}}$ ) that corresponds to the ground state ( $\min \bar{y}$ ) of a given QUBO, as the following equation [35, 37]:

$$\bar{\mathbf{x}} = \arg \min_{\mathbf{x}} \bar{y} \quad (1)$$

$$\bar{y} = \sum_{\mathbf{x}_i \in \{0,1\}^n} \mathbf{x}^T \mathbf{Q} \mathbf{x} \quad (2)$$

Here,  $\mathbf{Q}$  and  $\mathbf{x}$  denote a QUBO matrix and binary vector, respectively.  $\bar{y}$  indicates the energy state of a QUBO with a given  $\mathbf{x}$ . Various approaches have been proposed to address QUBO problems. Among them, QAOA, working with gate-based quantum computing, has demonstrated its potential to accelerate solving these optimization problems compared to its classical counterparts [18].

### 4.2 Building QUBOs

To solve optimization problems for material design using quantum computing, surrogates need to be defined with QUBO formulations, which describe the relationship between material structures and their FOMs. In this study, factorization machine (FM), a supervised learning algorithm, is used as a surrogate model to build QUBOs that represent optimization problems. FM efficiently learns the relationship between input binary vectors  $\mathbf{x}$  and corresponding output values  $y$  within a training dataset by the following equation [36, 33, 35]:

$$y = w_0 + \sum_{i=1}^n w_i x_i + \frac{1}{2} \sum_{f=1}^m \left[ \left( \sum_{i=1}^n v_{i,f} x_i \right)^2 - \sum_{i=1}^n v_{i,f}^2 x_i^2 \right] \quad (3)$$

Here,  $n$  is the length of the input binary vector  $\mathbf{x}$ , and  $m$  denotes the latent space size. The length of the input vector is denoted as the problem size  $n$  (i.e., QUBO size,  $n \times n$  matrix). FM model parameters ( $w_0$ ,  $w_i$ , and  $v_{i,f}$ ) can be obtained after training, where  $w_0$ ,  $w_i$ , and  $v_{i,f}$  respectively indicate a global bias, a linear coefficient for self-interaction, and a quadratic coefficient for pairwise interactions between features. These model parameters are directly mapped to a QUBO model, which serves as a surrogate by describing the relationship between material structures and their FOMs.

To analyze the performance of QAOA and DQAOA, we generate QUBO problems after training FM with datasets that depict the relationship between material structures (spectral filters) and their calculated FOMs. Hence, these QUBO matrices are large and dense (Fig. S5), reflecting real-world optimization scenarios. In this study, the QUBO

size (i.e., the length of a binary bit string representing a material structure) ranges from 6 to 1,000, indicating 6-bit to 1,000-bit problems.

### 4.3 QUBO decomposition

Large QUBO problems are hard to solve with current conventional quantum technologies. Therefore, we decompose a large QUBO into smaller sub-QUBOs and aggregate sub-solutions from the sub-QUBOs to obtain a global solution. This decomposition strategy greatly reduces the complexity of handling a large QUBO. For example, a QUBO problem with 8 decision variables involves 8 self-interactions and 28 pairwise interactions. By fixing 3 decisions and decomposing the QUBO into several sub-QUBOs with 5 decisions each, we can reduce the complexity of each sub-QUBO to have 5 self-interactions and 10 interactions (Fig. 1c), making it more suitable for current quantum computing systems. This QUBO decomposition can find a true global optimal solution of an original large QUBO when preserving essential structure and interactions of the original problem [43, 44]. However, it can be computationally expensive and ineffective to solve all sub-QUBOs to identify the global optimal solution, especially for large-scale problems due to the exponential number of possible combinations  ${}_nC_k$ . Here,  $n$  and  $k$  represent the size of the original QUBO and sub-QUBOs, respectively. Hence, our algorithm iterates the decomposition and aggregate processes with randomly selected sub-QUBOs among the whole possibilities. Then, sub-QUBOs are solved using DQAOA.

### 4.4 DQAOA

DQAOA can operate on both single-core and multi-cores/nodes within HPC-QC integrated systems. Our algorithm is tested on the Frontier supercomputer at the Oak Ridge Leadership Computing Facility, which is equipped with 64-core AMD “Optimized 3rd Gen EPYC” CPUs and 512 GB of memory per compute node [45]. In addition, each core interfaces with quantum systems (specifically, Qiskit Aer simulator in this study). dq-QAOA runs with a single core while DQAOA exploits multiple cores and nodes depending on the problem size. In this work, we use 50 cores per node, meaning that 150-bit problems would require 150 cores across 3 compute nodes. Distributed tasks across multi-cores and nodes are achieved by a message passing interface (MPI) implementation using mpi4py, enabling the simultaneous handling of numerous sub-QUBOs in each iteration [46].

### 4.5 AL-DQAOA

Our AL-DQAOA consists of three key components:

**(1) Factorization Machine:** FM is trained with a dataset to construct a QUBO model that serves as a surrogate by describing the correlation between material structures and their FOMs.

**(2) DQAOA:** DQAOA is employed to identify the approximated optimal binary state corresponding to the ground state of a QUBO model, which is formulated with the FM model parameters.

**(3) Wave-Optics Simulation:** The optical properties of the approximated optimal material state obtained from DQAOA (in step 2) are evaluated to calculate a FOM. Here, we use TMM for evaluating the optical properties of the designed materials, but other types of simulation tools can be used for different purposes.

The dataset is updated by adding the identified optimal binary state (from step 2) and the calculated FOM (from step 3). Iterating these processes improves the dataset quality, enabling FM to build a more reliable surrogate. Subsequently, DQAOA can discover a higher-quality data point, which leads to the convergence toward the optimal state in a global optimization space as iterations progress (see Fig. S7). DQAOA can select the same binary vector that was already identified in a previous optimization cycle. In this scenario, a randomly generated binary vector (i.e., random material structure) and its calculated FOM are added for updating the dataset instead of those obtained from DQAOA to avoid redundancy and increase diversity in the dataset (red dots in Figs. S7 and S9).

We first generate an initial dataset that includes 25 random photonic structures and their calculated FOMs, and start optimization with AL-DQAOA. Before training FM, we split a dataset into a training set and a test set in a 4:1 ratio. Random structures are increasingly added to the dataset, meaning that DQAOA identifies the repeated structures, when the convergence is almost reached. In addition, the convergence is usually achieved within several thousands of optimization cycles, depending on the problem sizes. Upon reaching convergence, AL-DQAOA usually does not find higher-quality data points [33, 35]. Therefore, we stop iterations upon satisfying preset thresholds to save computational costs: (1) 90 data out of the last 100 optimization cycles are from random structures, which indicates that the convergence is nearly achieved. (2) The number of optimization cycles reaches 3,000, 4,000, and 5,000 for 30-bit, 50-bit, and 100-bit problems, respectively. Given these strategies and thresholds, we can successfully optimize material structures (in this study, spectral filters as examples), featuring significantly large optimization spaces up to  $2^{100}$ .

## 4.6 Optimal Design of Spectral Filters using AL-DQAOA

We apply our AL-DQAOA to optimize spectral filters, and our goal is to optimally design spectral filters for high transmission in the visible spectrum while attenuating transmission in the ultraviolet (UV) and near-infrared (NIR) regions. Additionally, a thermal radiative polymer layer is added on the top of the filter surface, focusing on their application in the transparent radiative cooler (TRC). [33]. TRC has attracted a lot of interest recently due to its potential to address the global warming issue by reducing cooling energy consumption [42, 40, 33]. This energy-saving capability comes from the distinct

optical properties of the designed spectral filter to reflect heat-generating photons (UV and NIR photons) while selectively transmitting visible light. Additionally, the polymer layer on the top emits thermal radiation through the atmospheric window [39].

We design planar multilayered structures (PML) for spectral filters (Fig. 4b). The PML consists of 3 to 50 layers (total thickness is 1,200 nm), and each layer is composed of one of four material candidates: silicon dioxide:  $\text{SiO}_2$ , silicon nitride:  $\text{Si}_3\text{N}_4$ , aluminum oxide:  $\text{Al}_2\text{O}_3$ , and titanium dioxide:  $\text{TiO}_2$ . With each layer represented by a two-digit binary label (‘00’ for  $\text{SiO}_2$ , ‘01’ for  $\text{Si}_3\text{N}_4$ , ‘10’ for  $\text{Al}_2\text{O}_3$ , and ‘11’ for  $\text{TiO}_2$ ), a layer configuration can be described by a binary vector. Here, optimizing  $nl$ -layered spectral filters represents  $2nl$ -bit optimization problems, thus optimizing 50-layered spectral filters represents a 100-bit optimization problem. For example, a 6-layered structure composed of  $\text{SiO}_2/\text{Si}_3\text{N}_4/\text{Al}_2\text{O}_3/\text{TiO}_2/\text{Al}_2\text{O}_3/\text{Si}_3\text{N}_4$  is represented as [00 01 10 11 10 01]. Spectral filters for TRC can be realized by adding 40  $\mu\text{m}$  of polydimethylsiloxane layer on the top of the PML. The ideal spectral filter (i.e., ideal TRC) should have unity transmission in the visible regime and zero transmission in the UV/NIR regimes, resulting in a high solar-weighted transmission (i.e., transmitted solar irradiance) in the visible range and zero in other ranges. The objective is to align the optical properties of the designed spectral filters as closely as possible with these ideal properties in terms of transmitted irradiance. To evaluate the performance of the designed spectral filters, we calculate the FOM using the following equation:

$$\text{FOM} = \frac{10 \int_{\lambda=300}^{\lambda=2,500} [(T_{ideal}(\lambda)S(\lambda))^2 - (T_{designed}(\lambda)S(\lambda))^2] d\lambda}{\int_{\lambda=300}^{\lambda=2,500} S(\lambda)^2 d\lambda} \quad (4)$$

In this equation,  $S(\lambda)$  is the solar irradiance,  $T_{designed}(\lambda)$  and  $T_{ideal}(\lambda)$  indicate the transmission efficiency of a designed and ideal spectral filter, respectively.  $T(\lambda)S(\lambda)$  denotes the transmitted irradiance. The optical properties ( $T_{designed}(\lambda)$ ) are calculated using the transfer matrix method, a highly effective optical simulation tool for multilayered structures [33, 35, 38]. It is important to note that this represents a minimization optimization problem, as the FOM approaches 0 when the spectral filter exhibits high performance having optical properties similar to the ideal one.

## Acknowledgments

This research used resources of the Oak Ridge Leadership Computing Facility at the Oak Ridge National Laboratory, which is supported by the Office of Science of the U.S. Department of Energy under Contract No. DE-AC05-00OR22725. *Notice:* This manuscript has in part been authored by UT-Battelle, LLC under Contract No. DE-AC05-00OR22725 with the U.S. Department of Energy. The United States Government retains and the publisher, by accepting the article for publication, acknowledges that the U.S. Government retains a non-exclusive, paid up, irrevocable, world-wide license to publish

or reproduce the published form of the manuscript, or allow others to do so, for U.S. Government 15 purposes. The Department of Energy will provide public access to these results of federally sponsored research in accordance with the DOE Public Access Plan (<http://energy.gov/downloads/doe-publicaccess-plan>).

## Data availability

All data generated and analyzed during the study are available from the corresponding author upon reasonable request.

## Code availability

The codes used for generating and analyzing data are available from the corresponding author upon reasonable request.

## Author information

Authors and Affiliations:

**National Center for Computational Sciences, Oak Ridge National Laboratory, Oak Ridge, Tennessee 37830, United States.**

Seongmin Kim & In-Saeng Suh

**Department of Aerospace and Mechanical Engineering, University of Notre Dame, Notre Dame, Indiana 46556, United States**

Tengfei Luo

**Department of Electronic Engineering, Kyung Hee University, Yongin-Si, Gyeonggi-do 17104, Republic of Korea**

Eungkyu Lee

## Contributions

S.K. and I.S. conceived the idea and designed the experiments. S.K. developed the codes, derived all experimental results, and performed data analyses. All authors discussed the results, and contributed to the writing of the manuscript.

## Corresponding authors

Correspondence to In-Saeng Suh, Eungkyu Lee, Tengfei Luo, and Seongmin Kim.

Email address: In-Saeng Suh ([suhi@ornl.gov](mailto:suhi@ornl.gov)), Eungkyu Lee ([eleest@khu.ac.kr](mailto:eleest@khu.ac.kr)), Tengfei Luo ([tluo@nd.edu](mailto:tluo@nd.edu)), and Seongmin Kim ([kims@ornl.gov](mailto:kims@ornl.gov)).

# Ethics declarations

## Competing Interests

The authors declare no competing interests.

## References

- [1] Graham, T. *et al.* Multi-qubit entanglement and algorithms on a neutral-atom quantum computer. *Nature* **604**, 457–462 (2022).
- [2] Daley, A. J. *et al.* Practical quantum advantage in quantum simulation. *Nature* **607**, 667–676 (2022).
- [3] Huang, H.-Y. *et al.* Quantum advantage in learning from experiments. *Science* **376**, 1182–1186 (2022).
- [4] Arute, F. *et al.* Quantum supremacy using a programmable superconducting processor. *Nature* **574**, 505–510 (2019).
- [5] Sels, D., Dashti, H., Mora, S., Demler, O. & Demler, E. Quantum approximate bayesian computation for nmr model inference. *Nature machine intelligence* **2**, 396–402 (2020).
- [6] Abbas, A. *et al.* The power of quantum neural networks. *Nature Computational Science* **1**, 403–409 (2021).
- [7] Bernstein, D. J. & Lange, T. Post-quantum cryptography. *Nature* **549**, 188–194 (2017).
- [8] Bauer, B., Bravyi, S., Motta, M. & Chan, G. K.-L. Quantum algorithms for quantum chemistry and quantum materials science. *Chemical Reviews* **120**, 12685–12717 (2020).
- [9] Ren, W. *et al.* Experimental quantum adversarial learning with programmable superconducting qubits. *Nature Computational Science* **2**, 711–717 (2022).
- [10] West, M. T. *et al.* Towards quantum enhanced adversarial robustness in machine learning. *Nature Machine Intelligence* **5**, 581–589 (2023).
- [11] FÜRrutter, F., Muñoz-Gil, G. & Briegel, H. J. Quantum circuit synthesis with diffusion models. *Nature Machine Intelligence* 1–10 (2024).
- [12] Bernal, D. E. *et al.* Perspectives of quantum computing for chemical engineering. *AIChE Journal* **68**, e17651 (2022).

- [13] Akahoshi, Y., Maruyama, K., Oshima, H., Sato, S. & Fujii, K. Partially fault-tolerant quantum computing architecture with error-corrected clifford gates and space-time efficient analog rotations. *PRX Quantum* **5**, 010337 (2024).
- [14] Farhi, E. & Harrow, A. W. Quantum supremacy through the quantum approximate optimization algorithm (2019). URL <https://arxiv.org/abs/1602.07674>. 1602.07674.
- [15] Bittel, L. & Kliesch, M. Training variational quantum algorithms is np-hard. *Physical review letters* **127**, 120502 (2021).
- [16] Cerezo, M. *et al.* Variational quantum algorithms. *Nature Reviews Physics* **3**, 625–644 (2021).
- [17] Lykov, D. *et al.* Sampling frequency thresholds for the quantum advantage of the quantum approximate optimization algorithm. *npj Quantum Information* **9**, 73 (2023).
- [18] Shaydulin, R. *et al.* Evidence of scaling advantage for the quantum approximate optimization algorithm on a classically intractable problem. *Science Advances* **10**, eadm6761 (2024).
- [19] Zhou, Z., Du, Y., Tian, X. & Tao, D. Qaoa-in-qaoa: solving large-scale maxcut problems on small quantum machines. *Physical Review Applied* **19**, 024027 (2023).
- [20] Van Dam, W., Eldefrawy, K., Genise, N. & Parham, N. Quantum optimization heuristics with an application to knapsack problems. In *2021 IEEE International Conference on Quantum Computing and Engineering (QCE)*, 160–170 (IEEE, 2021).
- [21] Zhou, L., Wang, S.-T., Choi, S., Pichler, H. & Lukin, M. D. Quantum approximate optimization algorithm: Performance, mechanism, and implementation on near-term devices. *Physical Review X* **10**, 021067 (2020).
- [22] Brandhofer, S. *et al.* Benchmarking the performance of portfolio optimization with qaoa. *Quantum Information Processing* **22**, 25 (2022).
- [23] Pellow-Jarman, A. *et al.* The effect of classical optimizers and ansatz depth on qaoa performance in noisy devices. *Scientific Reports* **14**, 16011 (2024).
- [24] Preskill, J. Quantum computing in the nisc era and beyond. *Quantum* **2**, 79 (2018).
- [25] De Leon, N. P. *et al.* Materials challenges and opportunities for quantum computing hardware. *Science* **372**, eabb2823 (2021).
- [26] Bennewitz, E. R., Hopfmueller, F., Kulchytskyy, B., Carrasquilla, J. & Ronagh, P. Neural error mitigation of near-term quantum simulations. *Nature Machine Intelligence* **4**, 618–624 (2022).

- [27] Lykov, D., Shaydulin, R., Sun, Y., Alexeev, Y. & Pistoia, M. Fast simulation of high-depth qaoa circuits. In *Proceedings of the SC'23 Workshops of The International Conference on High Performance Computing, Network, Storage, and Analysis*, 1443–1451 (2023).
- [28] DeCross, M., Chertkov, E., Kohagen, M. & Foss-Feig, M. Qubit-reuse compilation with mid-circuit measurement and reset. *Physical Review X* **13**, 041057 (2023).
- [29] Kim, S. & Suh, I.-S. Performance analysis of an optimization algorithm for metamaterial design on the integrated high-performance computing and quantum systems. *arXiv preprint arXiv:2405.02211* (2024).
- [30] Britt, K. A. & Humble, T. S. High-performance computing with quantum processing units. *ACM Journal on Emerging Technologies in Computing Systems (JETC)* **13**, 1–13 (2017).
- [31] Humble, T. S. *et al.* Quantum computers for high-performance computing. *IEEE Micro* **41**, 15–23 (2021).
- [32] Date, P., Arthur, D. & Pusey-Nazzaro, L. Qubo formulations for training machine learning models. *Scientific reports* **11**, 10029 (2021).
- [33] Kim, S. *et al.* High-performance transparent radiative cooler designed by quantum computing. *ACS Energy Letters* **7**, 4134–4141 (2022).
- [34] Kim, S., Wu, S., Jian, R., Xiong, G. & Luo, T. Design of a high-performance titanium nitride metastructure-based solar absorber using quantum computing-assisted optimization. *ACS Applied Materials & Interfaces* **15**, 40606–40613 (2023).
- [35] Kim, S., Jung, S., Bobbitt, A., Lee, E. & Luo, T. Wide-angle spectral filter for energy-saving windows designed by quantum annealing-enhanced active learning. *Cell Reports Physical Science* (2024).
- [36] Kitai, K. *et al.* Designing metamaterials with quantum annealing and factorization machines. *Physical Review Research* **2**, 013319 (2020).
- [37] Kim, S. *et al.* Quantum annealing-aided design of an ultrathin-metamaterial optical diode. *Nano Convergence* **11**, 1–11 (2024).
- [38] Luce, A., Mahdavi, A., Marquardt, F. & Wankerl, H. Tmm-fast, a transfer matrix computation package for multilayer thin-film optimization: tutorial. *JOSA A* **39**, 1007–1013 (2022).
- [39] Zhu, B. *et al.* Subambient daytime radiative cooling textile based on nanoprocessed silk. *Nature nanotechnology* **16**, 1342–1348 (2021).

- [40] Kim, M. *et al.* Visibly transparent radiative cooler under direct sunlight. *Advanced Optical Materials* **9**, 2002226 (2021).
- [41] Li, T. *et al.* A radiative cooling structural material. *Science* **364**, 760–763 (2019).
- [42] Wang, S. *et al.* Scalable thermochromic smart windows with passive radiative cooling regulation. *Science* **374**, 1501–1504 (2021).
- [43] Glover, F., Kochenberger, G. & Du, Y. Quantum bridge analytics i: a tutorial on formulating and using qubo models. *Ijor* **17**, 335–371 (2019).
- [44] Atobe, Y., Tawada, M. & Togawa, N. Hybrid annealing method based on subqubo model extraction with multiple solution instances. *IEEE Transactions on Computers* **71**, 2606–2619 (2021).
- [45] Budiardja, R. D. *et al.* Ready for the frontier: Preparing applications for the world’s first exascale system. In *International Conference on High Performance Computing*, 182–201 (Springer, 2023).
- [46] Dalcin, L. D., Paz, R. R., Kler, P. A. & Cosimo, A. Parallel distributed computing using python. *Advances in Water Resources* **34**, 1124–1139 (2011).

# Supplementary Information

## Supplementary Note 1. Quantum Approximate Optimization Algorithm

We utilize the Quantum Approximate Optimization Algorithm (QAOA) to solve optimization problems that are formulated as quadratic unconstrained binary optimization (QUBO) models [1, 2]. We use conventional libraries to generate and solve quantum circuits for QAOA, such as 'qiskit (version 0.41.0)' and 'qiskit-optimization (version 0.4.0)' [3]. We use the QuadraticProgram to represent optimization problems from QUBOs, COBYLA optimizer as a classical optimizer for QAOA, and MinimumEigenOptimizer to approximate the ground state of Hamiltonian. After defining the backend (here, we use the Aer simulator (version 0.11.2) with the 'automatic' method), this variational quantum algorithm can approximate the ground state of the given QUBO problems and return the corresponding binary state. QAOA is generally effective in finding the true ground state and its binary state if the problem size is small enough (less than 16 according to our study); however, it struggles to solve larger problems, resulting in low accuracy and long time-to-solution [4]. It should be noted that the performance can be improved by using advanced QAOA algorithms and quantum systems. We emphasize that our distributed QAOA (DQAOA) will have an even higher performance by adopting those advanced technologies, which will be our future work.

## Supplementary Note 2. Number of Sub-QUBOs and Cores Used for DQAOA

The number of sub-QUBOs<sub>init</sub> in the initialization step is  $n-k+1$ , where  $n$  is the size of the original QUBO and  $k$  is the size of sub-QUBOs. These initial sub-QUBOs are generated with a linear sequence. For instance, sub-QUBO<sub>init,1</sub> includes 1<sup>st</sup> to 4<sup>th</sup> decisions, sub-QUBO<sub>init,2</sub> includes 2<sup>nd</sup> to 5<sup>th</sup> decisions, sub-QUBO<sub>init,3</sub> includes 3<sup>rd</sup> to 6<sup>th</sup> decisions, and sub-QUBO<sub>init,n-k+1</sub> includes  $(n-k+1)^{th}$  to  $n^{th}$  decisions (Fig. S1a). Hence, the number of cores used for DQAOA should be larger than  $n-k+1$  to distribute each sub-task (from sub-QUBO<sub>init,1</sub> to sub-QUBO<sub>init,n-k+1</sub>) across cores (50 cores per compute node). Meanwhile, the number of sub-QUBOs in the iteration step ( $b$ ) is decided by the number of cores used in DQAOA, where each core handles one sub-QUBO (Fig. S1b). dq-QAOA employs a single core, thus it can handle only one sub-QUBO in an iteration step. Consequently, dq-QAOA requires much more iterations than DQAOA.

## Supplementary Note 3. Performance Analysis

We analyze the performance of QAOA, dq-QAOA, and DQAOA by examining accuracies and time-to-solutions for given QUBO problems. We utilize a hybrid quantum annealing (HQA) method developed by D-Wave Systems (Advantage 4.1), which is specially developed for solving optimization problems, to determine the best-approximated ground state of QUBO problems ( $n=6$  to 1,000) [5, 6]. The operational principle of this quantum

system is based on quantum annealing, where the system evolves towards the ground state of the given problem through the quantum adiabatic process [7, 8, 9]. This principle is fundamentally different from that of gate-based quantum computing systems, but HQA is known as the best QUBO solver with the highest accuracy to date. We evaluate the accuracies by comparing solutions obtained from QAOA, dq-QAOA, and DQAOA with those obtained from HQA:

$$\text{Accuracy} = \frac{\text{Solution}_{\text{QAOA or DQAOA}}}{\text{Solution}_{\text{HQA}}} \quad (1)$$

We obtain time-to-solution by measuring the time to obtain a global solution by solving given QUBO problems from the job submission.

#### Supplementary Note 4. Expected Time to Complete Active Learning

We define the expected time required for completing active learning by the following equation:  $(\text{ML}_{\text{avg}} + \text{DQAOA}_{\text{avg}} + \text{TMM}_{\text{avg}}) \times \text{iterations}$ . Here, iterations vary depending on the optimization space size; we assume that 250, 2,000, 4,000, and 5,000 iterations are required to complete optimization for 12, 30, 50, and 100-bit systems, respectively. We note that the difference in time taken to solve QUBOs of DQAOA or dq-QAOA is the main factor causing the difference in the overall optimization time in active learning (AL-DQAOA); DQAOA requires 12.56, 20.03, 29.63, and 35.18 s for an iteration while dq-QAOA requires 37.92, 49.99, 59.35, and 73.58 s for 12, 30, 50, and 100-bit systems, respectively (see Figs. 4e and S8).

#### Supplementary Note 5. Energy Saving Calculation

EnergyPlus software (v9.4) is employed to calculate energy consumption for cooling in a standard office [10, 11], which has a dimension of 6 m (width)  $\times$  8 m (length)  $\times$  2.7 m (height) with two windows (3 m (width)  $\times$  2 m (height)). This office model is simulated with conventional windows or the designed transparent radiative cooling (TRC) windows using the software (Fig. S11a). The target cooling temperature is set to 24°C, and other settings are maintained at default values, except for optical properties specific to the optimized spectral filter used as TRC windows. Solar transmittance, solar reflectance, visible transmittance, visible reflectance, infrared transmittance, and hemispherical emittance for energy consumption calculation are 0.6738, 0.3262, 0.9196, 0.0804, 0.3908, and 0.5343, respectively, which are obtained from TMM.

Sixteen international cities in temperate or hot/tropical climates (Beijing, Berlin, Geneva, Incheon, London, Prague, Sapporo, Ulaanbaatar, Addis Ababa, Bangkok, Colombo, Harare, Havana, Lima, Phoenix, and Singapore) are selected to evaluate the energy consumption for cooling. Weather data for these cities are obtained from the EnergyPlus website [12, 13].

## Supplementary Figures

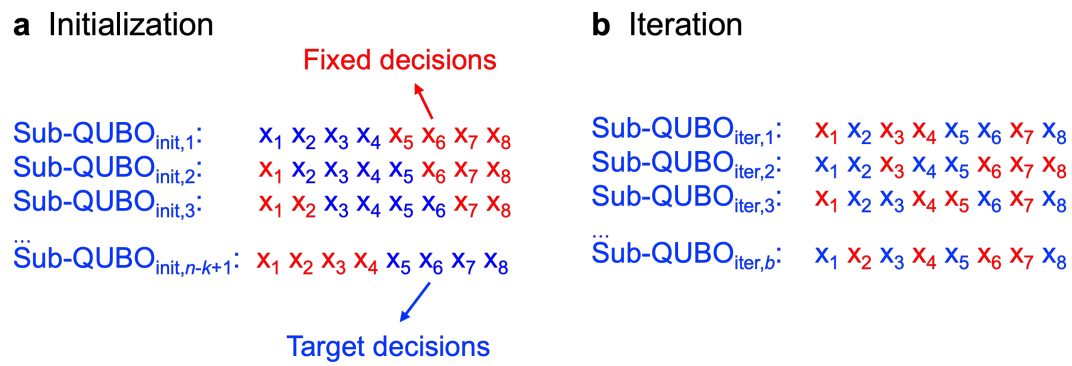


**Fig. 1: Generation of sub-QUBOs in DQAOA** for the (a) initialization step and (b) iteration step. In this example, the original QUBO size ( $n$ ) is 8, and the sub-QUBO size ( $k$ ) is 4. Note that the number of sub-QUBO for the iteration step is 1 for dq-QAOA (see Supplementary Note 2).

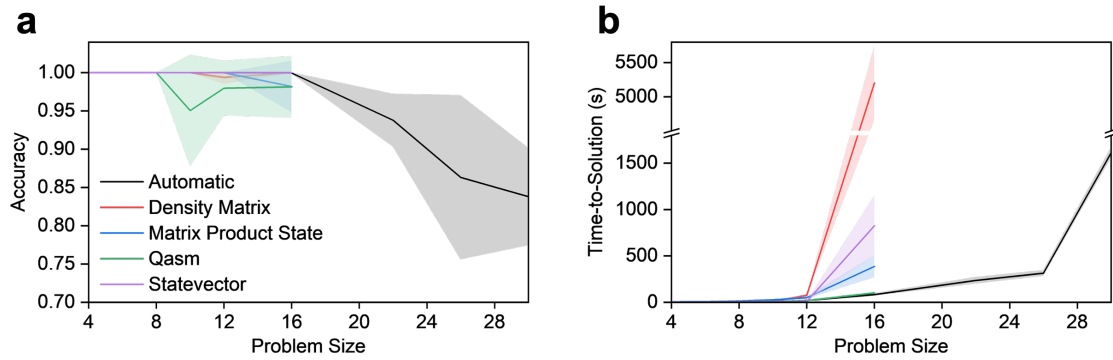


**Fig. 2:** Performance analysis of QAOA running with conventional quantum simulators (Qiskit Aer and BasicAer) with different methods (automatic, density matrix, matrix product state, qasm, and statevector). **a.** Accuracy and **b.** time-to-solution to solution for QUBO problems with different sizes.

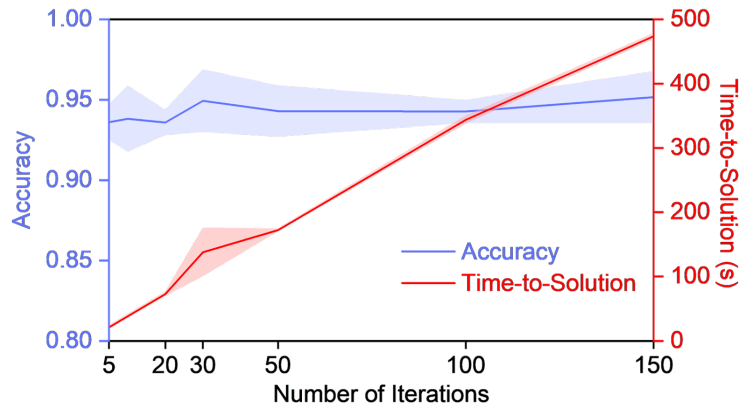


**Fig. 3:** Accuracy and time-to-solution of DQAOA for a 150-bit optimization problem as a function of the number of iterations. Here, the number of cores used is set to 150 and the sub-QUBO size to 8.

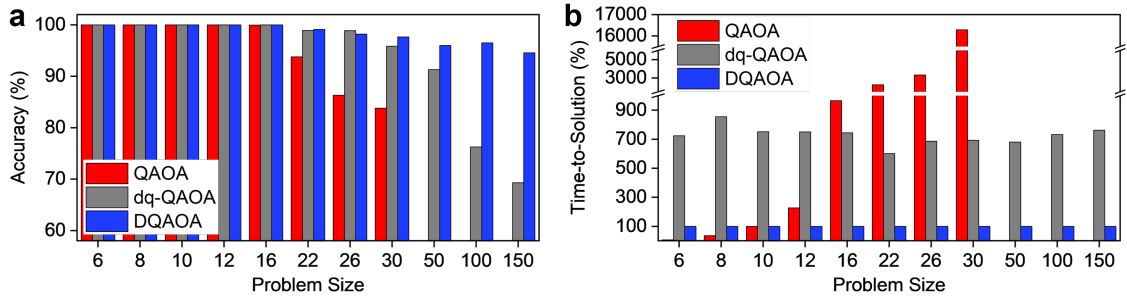


**Fig. 4: Performance analysis of QAOA, dq-QAOA, and DQAOA as a function of the problem size.** Comparison of (a) accuracy and (b) time-to-solution between QAOA, dq-QAOA, and DQAOA. The baseline for evaluating the accuracy is obtained from HQA, and the time-to-solutions are compared based on the time-to-solutions of DQAOA.

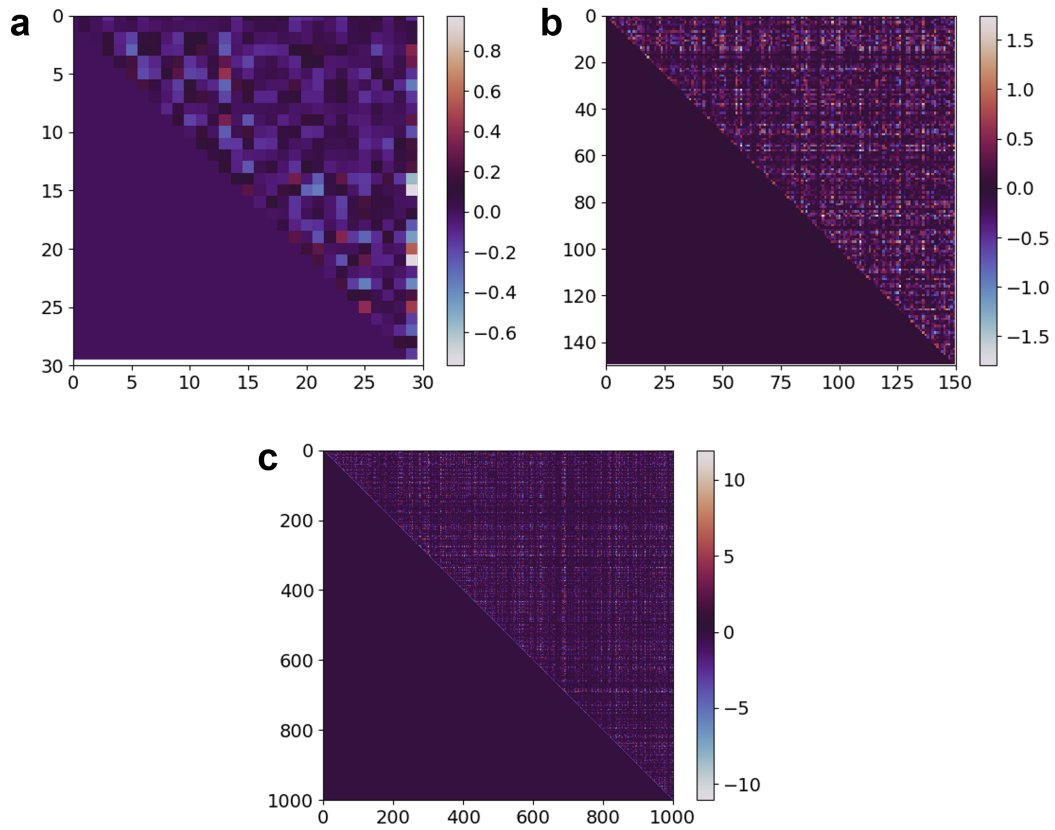


**Fig. 5:** QUBO matrices representing real-world optimization problems (spectral filters), which are large and dense. The problem size of the QUBO is (a) 30, (b) 150, and (c) 1000.

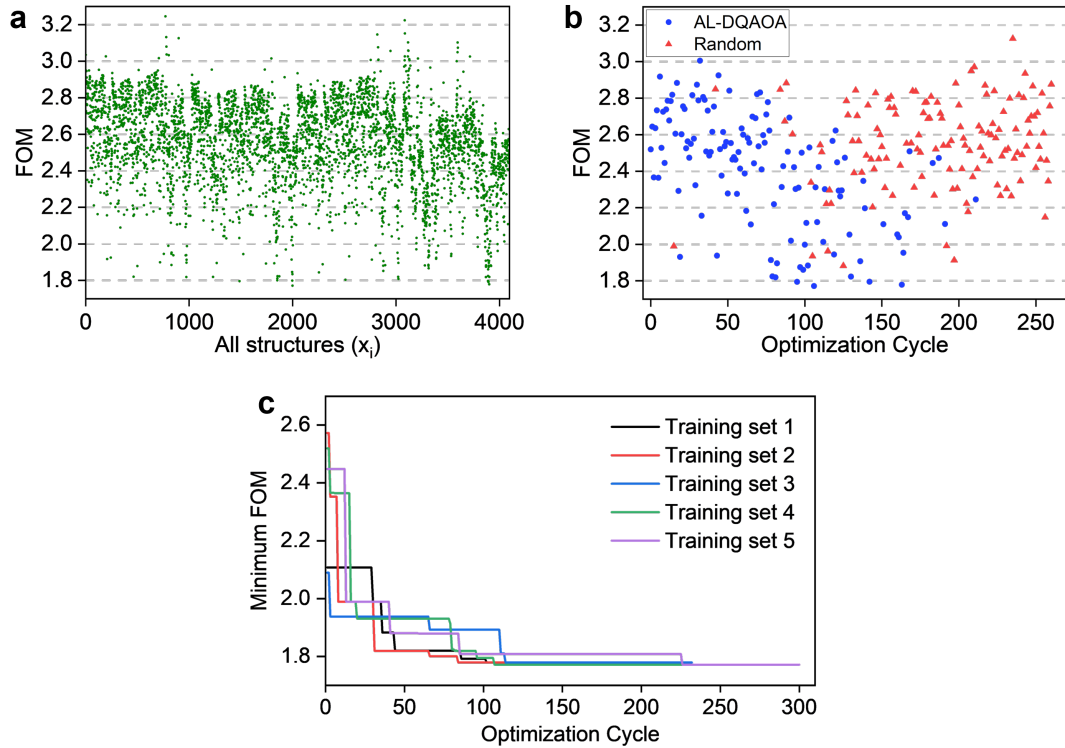


**Fig. 6: Benchmark study for the AL-DQAOA algorithm**, applied to a 6-layered spectral filter (representing a 12-bit optimization problem). **a.** Exhaustive enumeration of FOM for all possible structures. Among  $2^{12}$  ( $=4,096$ ) total possible structures, most structures have high FOM ( $>2.0$ ) and the FOM of an optimal structure is 1.7712. **b.** Optimization results using AL-DQAOA as a function of optimization cycles. AL-DQAOA identifies the global optimal structure within hundreds of optimization cycles. **c.** The evolution of FOM as a function of optimization cycles for different training sets, demonstrating convergence towards the global optimal point.

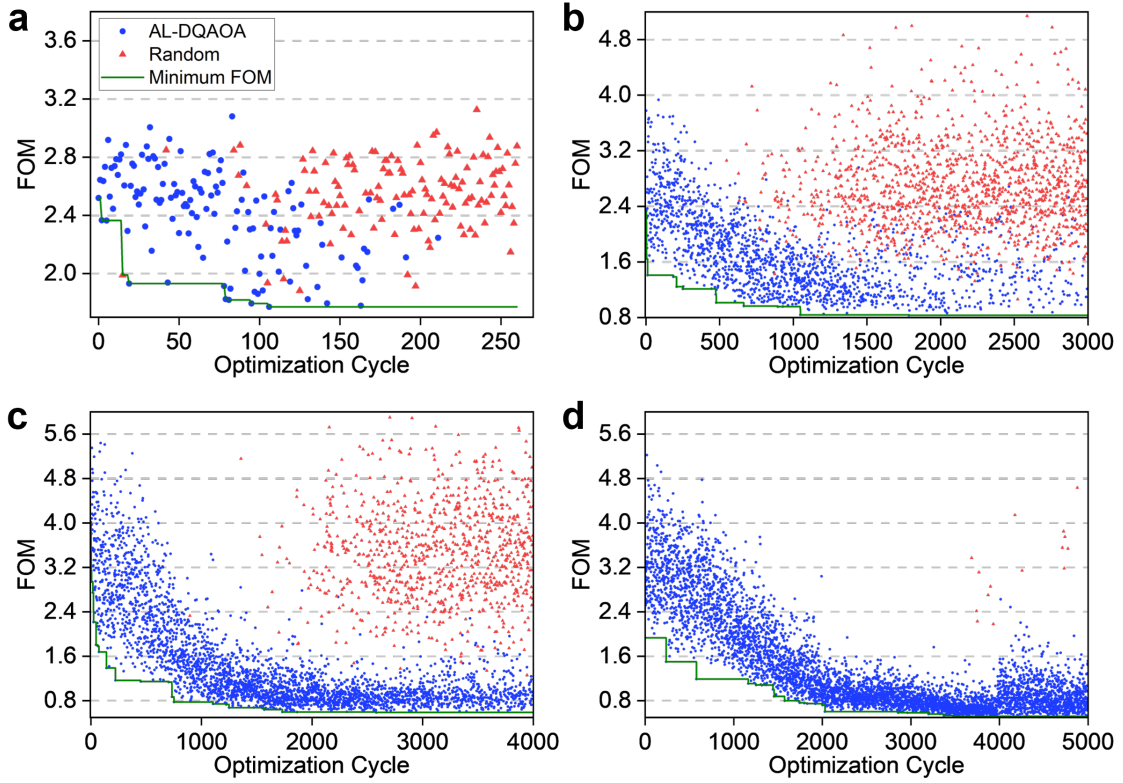


**Fig. 7: Optimization results using AL-DQAOA for different problem sizes.** FOM distribution and minimum FOM as a function of optimization cycles for (a) 12-bit (6-layered), (b) 30-bit (15-layered), (c) 50-bit (25-layered), and (d) 100-bit (50-layered) systems. The FOM distributions indicate that AL-DQAOA effectively identifies low FOMs as optimization cycles progress, with random structures generated after convergence is achieved. The results demonstrate that the convergence can be achieved within hundreds to thousands of optimization cycles, which is a very small fraction of the entire optimization space size (up to  $2^{100}$ ).

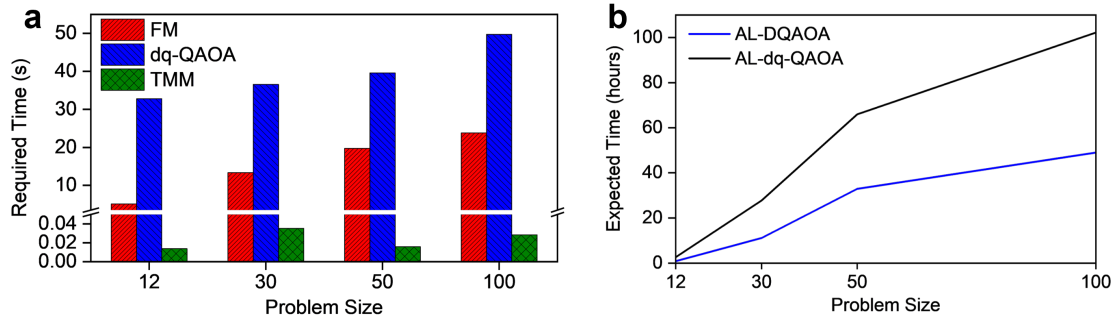


**Fig. 8: Required time for optimization using AL-DQAOA.** **a.** Time required for each optimization cycle of AL-dq-QAOA for different problem sizes. **b.** Expected time to complete active learning when using AL-DQAOA or AL-dq-QAOA for different problem sizes.

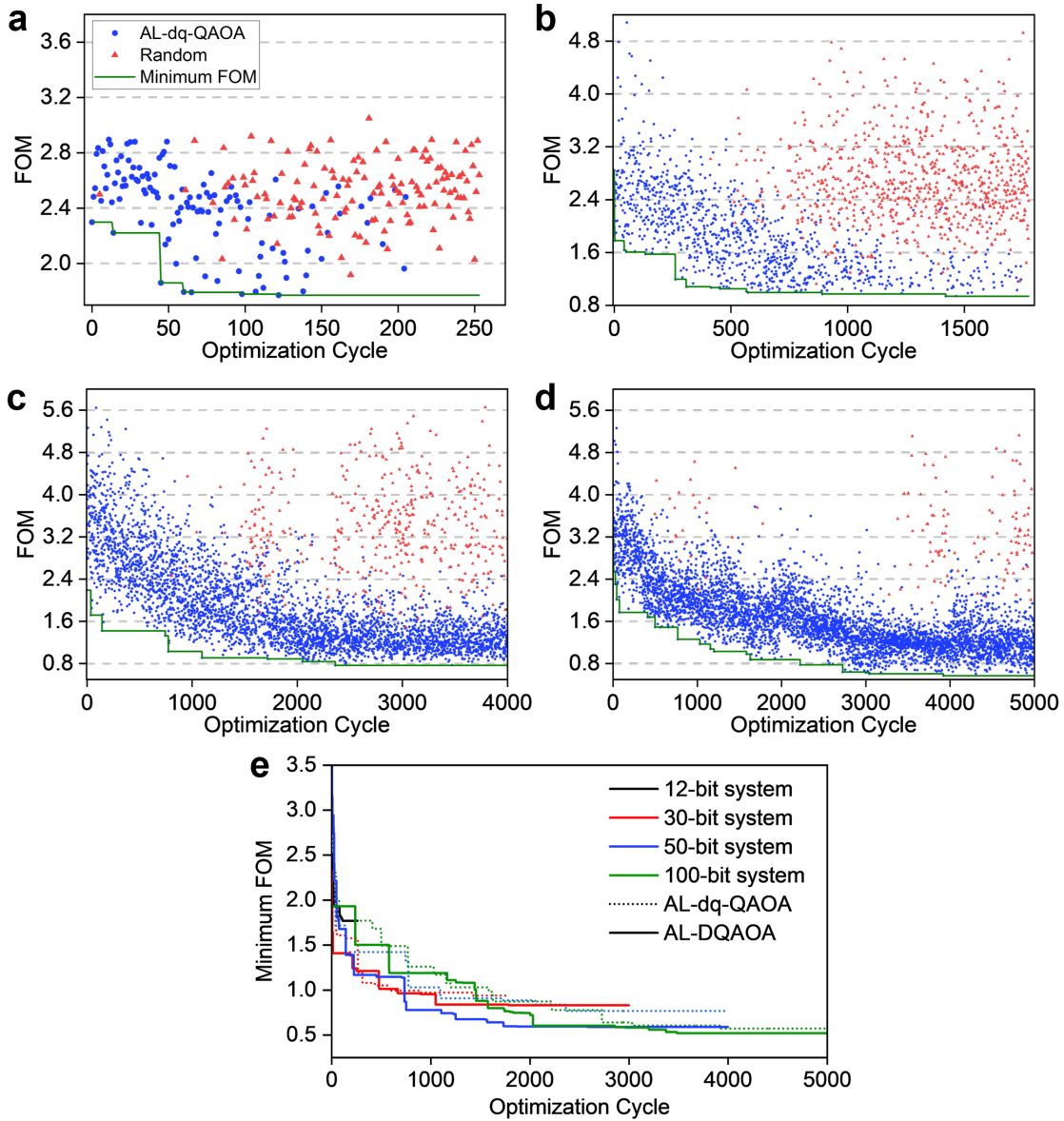


**Fig. 9: Optimization results using AL-dq-QAOA for different problem sizes.** FOM distribution and minimum FOM as a function of optimization cycles for (a) 12-bit (6-layered), (b) 30-bit (15-layered), (c) 50-bit (25-layered), and (d) 100-bit (50-layered) systems. e. The evolution of FOM as a function of optimization cycles for different problem sizes. Dashed and solid lines denote optimization results using AL-dq-QAOA and AL-DQAOA, respectively. AL-DQAOA consistently identifies better structures with lower FOMs than AL-dq-QAOA.

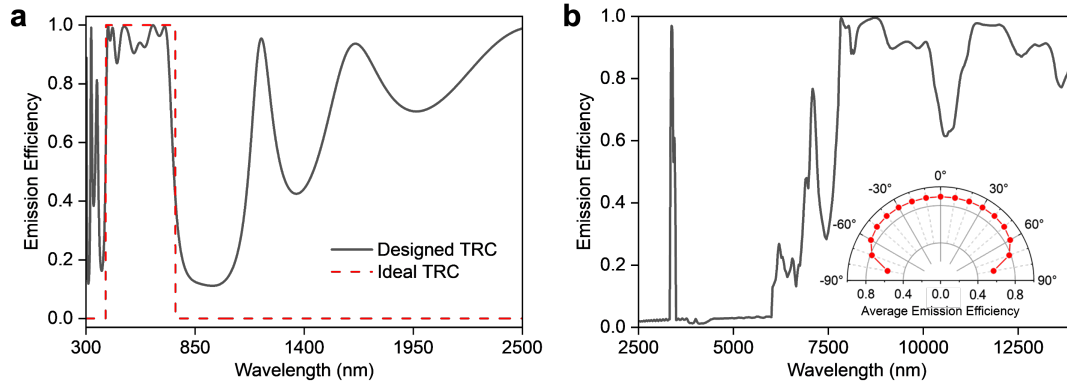


**Fig. 10: Optical properties of the spectral filter optimized by AL-DQAOA.**  
**a.** Transmission efficiency in the solar spectrum (wavelength: 300 to 2,500 nm). **b.** Emission efficiency in the mid and long-wavelength infrared range (wavelength: 2,500 to 14,200 nm). Inset: hemispherical emission efficiency in the atmospheric window range (wavelength: 8,000 to 13,000 nm).

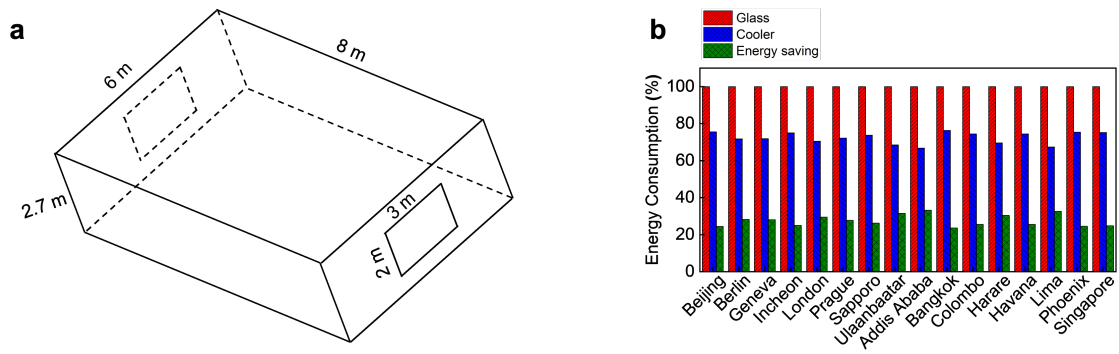


**Fig. 11: Energy-saving capability when using the optimized spectral filter as TRC windows. a.** Standard office model with two windows, used for calculating energy consumption for cooling. **b.** Calculated annual cooling energy consumption rate, compared to the cooling energy consumption of the office with conventional windows.

## References

- [1] Cerezo, M. *et al.* Variational quantum algorithms. *Nature Reviews Physics* **3**, 625–644 (2021).
- [2] Lykov, D. *et al.* Sampling frequency thresholds for the quantum advantage of the quantum approximate optimization algorithm. *npj Quantum Information* **9**, 73 (2023).
- [3] Qiskit: An open-source framework for quantum computing, (2019) .
- [4] Kim, S. & Suh, I.-S. Performance analysis of an optimization algorithm for metamaterial design on the integrated high-performance computing and quantum systems. *arXiv preprint arXiv:2405.02211* (2024).
- [5] Pastorello, D. & Blanzieri, E. Quantum annealing learning search for solving qubo problems. *Quantum Information Processing* **18**, 303 (2019).
- [6] Atobe, Y., Tawada, M. & Togawa, N. Hybrid annealing method based on subqubo model extraction with multiple solution instances. *IEEE Transactions on Computers* **71**, 2606–2619 (2021).
- [7] Somma, R. D., Nagaj, D. & Kieferová, M. Quantum speedup by quantum annealing. *Physical review letters* **109**, 050501 (2012).
- [8] Hibat-Allah, M., Inack, E. M., Wiersema, R., Melko, R. G. & Carrasquilla, J. Variational neural annealing. *Nature Machine Intelligence* **3**, 952–961 (2021).
- [9] Chen, Y.-Q., Chen, Y., Lee, C.-K., Zhang, S. & Hsieh, C.-Y. Optimizing quantum annealing schedules with monte carlo tree search enhanced with neural networks. *Nature Machine Intelligence* **4**, 269–278 (2022).
- [10] Li, T. *et al.* A radiative cooling structural material. *Science* **364**, 760–763 (2019).
- [11] Zhao, X. *et al.* A solution-processed radiative cooling glass. *Science* **382**, 684–691 (2023).
- [12] Kim, S., Jung, S., Bobbitt, A., Lee, E. & Luo, T. Wide-angle spectral filter for energy-saving windows designed by quantum annealing-enhanced active learning. *Cell Reports Physical Science* (2024).
- [13] Energyplus weather data. <https://energyplus.net/weather> .